Enhanced Photocatalytic Activity of Ce^{3+}-TiO_2 Hydrosols in Aqueous and Gaseous Phases

Tong-xu Liu[a,b], Xiang-zhong Li[a*], Fang-bai Li[b]

[a] *Department of Civil and Structural Engineering, The Hong Kong Polytechnic University, Kowloon, Hong Kong, China*

[b] *Guangdong Key Laboratory of Agricultural Environment Pollution Integrated Control, Guangdong Institute of Eco-Environment and Soil Science, Guangzhou 510650, PR China*

Abstract

A series of cerium ion-doped titanium dioxide (Ce^{3+}-TiO_2) hydrosols were prepared by a coprecipitation–peptization method and characterized by UV–Vis transmittance spectroscopy (T%), particle size distribution (PSD), X-ray diffraction (XRD), and Brunauer-Emmett-Teller (BET) and Barret-Joyner-Halender methods (BJH), respectively. The results demonstrated that as the doped Ce^{3+} content increased, the crystalline size, BET surface area and transmittance decreased significantly, but the particle size increased gradually. The photocatalytic activity of Ce^{3+}-TiO_2 hydrosols was evaluated in aqueous solution for methylene blue (MB) and 2,3-dichloriphenol (2,3-DCP) degradations, and also in gaseous phase for benzene degradation. The results showed that the overall photocatalytic activity of Ce^{3+}-TiO_2 hydrosols in aqueous and gaseous phases under UVA and visible illumination was significantly higher than pure TiO_2 hydrosol due to its better separation of electron-hole pairs and visible light response. Additionally, the formation surface-complex of TiO_2 and 2,3-DCP with visible-light-response is also contributed to the 2,3-DCP degradation, and the relevant possible reaction mechanisms were discussed with details. The kinetic data demonstrated that the Ce^{3+}-TiO_2 hydrosols with the content of Ce^{3+} doping between 0.5-1% achieved the best performance in both the aqueous and gaseous phases. This study provided the comprehensive understanding of the Ce^{3+}-TiO_2 hydrosol characteristics and reaction mechanisms, and the results indicate that these Ce^{3+}-TiO_2 hydrosols may have good potential for pollutant degradation either in aqueous phase or gaseous phase.

Keywords: *Ce^{3+}-TiO_2, Environmental Application, Hydrosols, Preparation, Photocatalytic Activity*

[*] *To whom correspondence should be addressed. Tel.: +852-27666016. Fax: +852-23346389. E-mail: cexzli@polyu.edu.hk*

1. Introduction

TiO_2 photocatalysis has become a promising technique for degrading aqueous or gaseous toxic organic pollutants in water and wastewater treatment, and air purification owing to its environmental benign [1, 2]. So far, a variety of physical and chemical approaches have succeeded in synthesizing crystalline TiO_2 catalysts by calcinations methods [3-5], while Xie et al. [6] synthesized the crystallized TiO_2 hydrosol at low temperature of < 100 °C by a hydrothermal method to avoid the serious aggregation by the calcinations methods. In comparison with the conventional TiO_2 powder catalysts, TiO_2 hydrosol is a colloidal solution with much finer TiO_2 particles and much better colloidal stability and homogeneity, and it can utilize the light more efficiently compared to those aqueous TiO_2 powder suspensions. Additionally, a key technique of using TiO_2 for indoor air purification is how to coat the catalysts such as P-25 powder onto walls, windows, or furniture easily and durably, without any blights such as color change and transparency decay of the substrates after coating, while using TiO_2 hydrosol can solve these problems because it is transparent and easy for coating on these substrates. Recently, only a few reports [7, 8] have directly used TiO_2 hydrosol to eliminate the air pollution under UV illumination, but there is still lack of the studies on the TiO_2 hydrosol for air purification under visible light illumination.

To further enhance the photocatalytic performance of TiO_2 hydrosols, some literatures have proved that the incorporation of lanthanide ion doping could improve the photochemical properties by increasing the photocurrent response and the separation of electron-hole pairs under UV illumination [9-13]. Some reports [14] showed the overall photocatalytic activity for 2-mercaptobenzothiazole degradation under UV or visible light irradiation was significantly enhanced by doping with the cerium ions with a special 4*f* electron configuration because the higher adsorption equilibrium constant and the higher separation efficiency of electron-hole pairs were obtained simultaneously for Ce^{3+}-TiO_2 powder catalysts and the introduction of Ce 4*f* level led to the optical absorption band between 400 and 500 nm, resulting its visible-induced photocatalytic activity. Xie et al. [15] reported Ce^{4+}–TiO_2 sol catalysts had photocatalytic activity for X-3B degradation under visible light irradiation, and they speculated the possible mechanisms. However, the photocatalytic activity of Ce^{3+}-TiO_2 hydrosol catalyst has only been studied with very limited data about dye degradation in aqueous solution. Especially, there is a lack of studies about its photocatalytic activity for degrading pollutants in gaseous phase. Recently, the development of non-

TiO_2 photocatalysts (such as β-Ga_2O_3, InOOH, and Zn_2GeO_4) [16] is one of the alternative approaches for treating gaseous benzene at ambient conditions, but these semiconductors usually have wide bandgap which should be excited by the light with the wavelength less than 300 nm. Comparatively, the Ce^{3+}-TiO_2 hydrosols with the ability of benzene degradation under UVA or visible light, is more suitable for the practical application, especially for the indoor air purification.

In this study, Ce^{3+}-TiO_2 hydrosol was prepared by using a chemical coprecipitation-peptization method and its colloidal properties and nanoparticle properties were characterized with details. The degradations of methyl blue (MB) and 2,3-dichlorophenol (2,3-DCP) with the Ce^{3+}-TiO_2 hydrosols in aqueous solution were first investigated and the degradations of benzene (C_6H_6) with the Ce^{3+}-TiO_2 hydrosols in gaseous phase were then conducted to evaluate its photocatalytic activity under UV or visible illumination. This study was aimed at investigating the enhanced photoactivity of Ce^{3+}-TiO_2 hydrosol photocatalyst for its environmental applications in aqueous and gaseous phases.

2. Experimental

2.1 Materials

Metatitanic acid ($TiO_2 \cdot 2.5H_2O \cdot 0.3SO_4$), a precursor of titania powder, was supplied from Panzhihua Iron & Steel Research Institute, China. While the MB and 2,3-DCP chemicals were obtained from BDH and Aldrich Chemical Company, respectively, NH_4OH, HNO_3, $Ce(NO_3)_3$ and other chemicals with analytical grade were obtained from Shanghai Reagent Ltd. The benzene gas with a certified concentration of 1,000 ppm/v in air was purchased from Foshan Kedi Gas Ltd. in China. Deionzied distilled water (DDW) was used for preparation of all solutions.

2.2 Preparation of Ce^{3+}-TiO_2 hydrosols

The Ce^{3+}-doped TiO_2 hydrosols were prepared by a chemical coprecipitation–peptization method, in which 90 g of metatitanic acid was added into DDW and stirred continuously until a uniform metatitanate suspension was obtained. 2.3 g of $Ce(NO_3)_3$ was dissolved into DDW to obtain cerium nitrate solution, which was then added into the metatitanate suspension and uniformly mixed. Excessive amount of ammonia was dropped therein to adjust the pH value to be above 9. The resulting suspension was stirred continuously for 3 h and heated at the temperature of below 40 °C, and then filtered to get filter cake. The filter cake was washed repeatedly for several times until no

sulfate ion was detected by titration using a 0.5 mol L^{-1} barium chloride solution. Finally, the filter cake was uniformly mixed with water to form uniform suspension. 190 mL of nitric acid (10%) was dropped therein to adjust the pH value to be 1.5. The resulting suspension was stirred continuously for 2 h at room temperature, followed by stirring and heating at the higher temperature of 65 °C. The suspension was peptized for 24 h to eventually obtain a Ce^{3+}-TiO_2 hydrosol solution in slight yellowish colour with a doped amount of cerium at 1.0% (mol/mol). This hydrosol sample was named "1.0%Ce^{3+}-TiO_2". With the same procedure, 0.5%Ce^{3+}, 1.5%Ce^{3+}, 2.0%Ce^{3+}, and 2.5%Ce^{3+} doping TiO_2 hydrosol samples were also prepared and named "0.5%Ce^{3+}-TiO_2", "1.0%Ce^{3+}-TiO_2", "1.5%Ce^{3+}-TiO_2", "2.0%Ce^{3+}-TiO_2", and "2.5%Ce^{3+}-TiO_2", respectively.

2.3 Characterization of Ce^{3+}-TiO_2 hydrosols

The as-prepared hydrosol samples were first scanned using a TU-1801 UV-visible spectrophotometer (UV-Vis TU-1800, Purkinje General, Beijing) in the wavelength range of 200-600 nm to determine their UV-visible transmittance spectra. The particle size distributions (PSD) of the hydrosols were directly determined by a light-scattering size analyzer (Beckman N5, USA). To characterize the crystalline and adsorption properties of the hydrosols, the titania xerogel powder was obtained through gelation treatment at 65 °C for 24 h. The X-ray powder diffraction (XRD) patterns were recorded using a Rigaku D/Max-III A diffractometer at room temperature with 30 kV and 30 mA under a Cu Kα radiation ($\lambda = 0.15418$ nm). The crystal sizes were calculated using the Scherrer's formula [17]. The specific surface area and total pore volume of hydrosol samples were measured by the Brunauer-Emmett-Teller (BET) method, in which the N_2 adsorption at 77 K using an ASAP 2020 Sorptometer was applied. The xerogel sample was degassed at 90 °C prior to nitrogen adsorption measurements. The pore size distribution was determined by the Barret-Joyner-Halender (BJH) method according to their desorption isotherm [18]. The nitrogen adsorption volume at the relative pressure (P/P_0) of 0.9733 was used to determine the pore volume and average pore sizes.

2.4 Photoreaction experiments

MB and 2,3-DCP chemicals were used as two model pollutants to evaluate the photocatalytic activity of the hydrosols in aqueous solution, while benzene was also tested to determine the photocatalytic activity of the hydrosols in gaseous phase.

Aqueous Phase Experiments. The photocatalytic reactions of MB/2,3-DCP degradation in aqueous solution were conducted in a Pyrex cylindrical photoreactor surrounded by a circulation water jacket to control the temperature during reaction. A medium-pressure mercury lamp (Philips, 8 W, 365 nm) was used as a UVA light source (I = 1.28 mW cm^{-2}), and a 300 W Xeon lamp (PLS-SXE300UV, Beijing Trusttech Ltd., China) with a UV cutoff filter at 420 nm was applied as a visible light source. The reaction mixture was prepared by adding hydrosol or P-25 powder into 250 mL of aqueous MB/2,3-DCP solution as colloid solution or powder suspension. In all experiments, the initial concentration of MB/2,3-DCP was 10 mg L^{-1} and the solid content of TiO_2 was 1.0 g L^{-1}. Prior to the photoreaction, the colloid solution/powder suspension was magnetically stirred in the dark for 30 min to establish adsorption/desorption equilibrium. During the photoreaction, the colloid solution or suspension was irradiated by UVA or visible light with air blowing and magnetically stirring. At the given time intervals, the samples were taken from the colloid solution or suspension and stored in the dark before analysis. The MB concentration was determined by a UV-Vis spectrophotometer at the wavelength of 665 nm. The 2,3-DCP concentration was determined by HPLC (Finnigan SpectraSYSTEM P4000) with a Pinnacle II C18 reverse-phase column (5 mm, 4.6 mm × 250 mm) and a UV detector (UV 6000LP) using all wavelength, in which a mobile phase was composed of acetonitrile and water (v:v = 3:2) and flowed at 1.0 mL min^{-1}.

Gaseous Phase Experiments. Gaseous benzene degradation was conducted in a stainless steel column reactor with an effective volume of 100 L (46 cm (D) × 60 cm (H)), which inner surface was coated with a Teflon film for eliminating adsorption. The reactor was placed in a small air chamber where temperature and humidity were well controlled. Inside of the reactor, three medium-pressure mercury lamps (Philips, 8 W) with the main emission at 365 nm or three fluorescent lamps (Philips, 8 W) with the main emissions at 405 nm, 430 nm, 540 nm, and 580 nm were equipped at the upper level as a UVA or visible light source and a TiO_2-coated sheet was placed on a Teflon film at the lower level horizontally about 1.5 cm below the lamps (I = 1.42 mW cm^{-2} for UV light, and 1.12 mW cm^{-2} for visible light). The TiO_2-coated sheet was prepared by spraying the hydrosol solution containing 0.5 g of TiO_2 onto a piece of filter paper (18 cm × 26 cm) to form a catalyst loading of 1.07 mg cm^{-2} and was then dried at 60 °C for 24 h before use. A synthetic benzene gas was prepared by mixing the certified benzene gas with zero air from cylinders with an initial benzene concentration of 5.5 ± 0.2 ppm/v. All the experiments were carried out at 25 ± 1 °C. The

humidity was controlled at 52 ± 2% by passing through a humidifier before photoreaction. The gaseous benzene concentration was determined using a benzene monitor (Ultra RAE, PGM-7200, USA), which has a measurement range of 0-10 ppm/v with a detection limit of 0.01 ppm/v.

3. Results and Discussion

3.1 The colloidal properties of Ce^{3+}-TiO_2 hydrosols

In this study, a pure TiO_2 hydrosol and a series of Ce^{3+}-TiO_2 hydrosols (0.5%Ce^{3+}-TiO_2, 1.0%Ce^{3+}-TiO_2, 1.5%Ce^{3+}-TiO_2, 2.0%Ce^{3+}-TiO_2, and 2.5%Ce^{3+}-TiO_2) were prepared, respectively, but it was found that not all samples were formed as good colloid solution. The detailed results are shown in Table 1.

[Table 1]

It can be seen that some stable hydrosols with a Ce^{3+} content up to 1.0% were obtained without any precipitates, while other hydrosols with a Ce^{3+} content at 1.5% or above contained some precipitates. The results showed that the higher content of Ce^{3+} doped into the TiO_2 hydrosols resulted in more precipitates and less sols in the sol solution. When the Ce^{3+} content reached 2.5%, no colloid solution could be formed at all. Furthermore, the transmittance spectra of hydrosols samples in Fig. 1 showed that the light transmittance decreased sharply as the Ce^{3+} content increased from 0% to 1.5%. Therefore, only four hydrosols (pure TiO_2, 0.5%Ce^{3+}-TiO_2, 1.0%Ce^{3+}-TiO_2, and 1.5%Ce^{3+}-TiO_2) were used in the following experiments.

[Fig. 1]

The PSD of the four hydrosols are presented in Fig. 2. The results demonstrated that all the hydrosol samples had a single-modal distribution characteristic with their PSD in the range of 15-50 nm. Furthermore, it was found that as the Ce^{3+} content increased, the PSD curves shifted to the right side, indicating that the main particle sizes of hydrosols became larger and the average particle sizes increased from 26.3 to 32.8 nm (Table 2). This could be the reason causing the decrease of light transmittance in the hydrosol solution with a high Ce^{3+} content.

[Fig. 2]

3.2 The structural properties of Ce^{3+}-TiO_2 hydrosols

The structural properties of the obtained Ce^{3+}-TiO_2 hydrosols were examined by the analyses of XRD, BET, and pore size distributions and the results are shown in Figs. 3 and 4.

XRD analysis. The XRD patterns of the TiO_2 and Ce^{3+}-TiO_2 hydrosols in Fig. 3 showed five distinctive TiO_2 peaks at 25.38°, 37.98°, 48.08°, 54.68° and 62.88°, corresponding to anatase (101), (004), (200), (105) and (204) crystal planes (JCPDS 21-1272), respectively. These results indicated that all the samples had anatase structure. The height of A (101) in Fig. 3 can denote the degree of the crystalline of various hydrosols, which was decreased gradually as the Ce^{3+} content increased from 0 to 1.5%. This decrease might indicate that the cerium ion doping inhibited the TiO_2 phase transfer from amorphous structure to anatase, and that Ce^{3+}-TiO_2 had higher thermal stability than pure TiO_2. Additionally, no cerium oxides peaks were found in the XRD grams because of a low cerium content [14].

[Fig. 3]

BET-BJH analysis. The effects of Ce^{3+} doping on the pore structure and adsorption ability of the TiO_2 catalyst were examined by the BET method, in which a set of N_2 adsorption/desorption isotherm tests was carried out and the experimental results are presented in Fig. 4a. The pore-size distribution of different catalysts was also determined by the BJH method and the results are shown in Fig. 4b. The adsorption isotherms in Fig. 4a showed the hysteresis loops of the Ce^{3+}-TiO_2 demonstrated a curve pattern between Type IV (BDDT classification) which exhibit hysteresis loops mostly of type H3 [18]. This indicates that the powders contain mesopores (2 – 50 nm) with narrow slit-like shapes or plate-like particles. It can be seen that all the adsorption capacity decreased gradually with the increase of Ce^{3+} content. The results in Fig. 4b demonstrated that the pore sizes of most catalysts were distributed in the range of 4 – 24 nm. But the peak of pore size distribution curves decreased sharply with the increase of Ce^{3+} content from 0 to 1.5%. Simultaneously, the data in Table 2 showed that both the BET surface area and pore volume decreased due to the increase of Ce^{3+} content, indicating the Ce^{3+} doping might occupy the porous

sites on the TiO_2 and result in lower surface area and smaller pore volume. These results seem to be matched with the PSD results but inconsistent with the XRD results. In fact, the ionic radii of Ce^{3+} and Ce^{4+} (1.03 and 1.02 Å) are much bigger than that of Ti^{4+} (0.64 Å). So it is difficult for Ce^{3+}/Ce^{4+} to enter the lattice of TiO_2 structure. These results showed that the amount of cerium ion on the surface of the Ce^{3+}-TiO_2 catalysts is higher that that in the bulk [19]. Hence, the cerium ion covered on the TiO_2 surface can inhabit the crystal growth of anatase to decrease crystal size, but can enhance the aggregation of colloidal particles to increase particle sizes.

[Fig. 4]

[Table 2]

3.3 Photocatalytic activity in aqueous phase

To evaluate the effects of Ce^{3+} content on the photocatalytic activity of Ce^{3+}-TiO_2 hydrosols in aqueous phase, two sets of tests for degradation of MB and 2,3-DCP in aqueous solutions under UV or visible illumination were conducted. The experimental results of MB and 2,3-DCP degradation with different catalysts under UVA illumination and visible illumination are shown in Figs. 5 and 6, respectively. To study the kinetics of MB and 2,3-DCP degradation in the aqueous phase, the pseudo-first-order model was applied to fit the experimental data and the kinetic reaction rate constants, *k*, versus cerium ion content are shown in Figs. 5c and 6c, respectively. The experimental results showed that the MB and 2,3-DCP degradations were considerably affected by the Ce^{3+} content. While the 0.5%Ce^{3+}-TiO_2 and 1.0%Ce^{3+}-TiO_2 hydrosols achieved the best performance in the MB and 2,3-DCP degradations under UVA illumination, 1.0% Ce^{3+}-TiO_2 and 0.5% Ce^{3+}-TiO_2 hydrosols achieved the best performance in the MB and 2,3-DCP degradations under visible illumination, respectively.

[Fig. 5]

[Fig. 6]

Under UVA illumination, our previous investigation [14] had proved that Ce^{3+} doping can accelerate the separation efficiency of charge carriers according to the photoluminescence emission

analysis. The Ce 4*f* level plays an important role in interfacial charge transfer and elimination of electron-hole recombination. Ce^{3+} ion could act as an effective electron scavenger to trap the conduction band electrons of TiO_2 and then photogenerated electrons were transferred efficiently. Hence, the enhanced activity of TiO_2 hydrosols under UVA illumination can be mainly attributed to the Ce^{3+}-induced higher separation efficiency of charge carriers. Under visible illumination, electron-hole pairs could be generated on either Ce^{3+}-TiO_2 or surface Ce_2O_3 as two approaches. Under visible light irradiation with the photon energy higher than ($E_{Ce4f} - E_v$), the electrons can be excited from the valence band of TiO_2 or the ground state of Ce_2O_3 into Ce 4*f* level to successfully separate the electron-hole pairs.

Furthermore, the visible response of Ce^{3+}-TiO_2 hydrosol was not just attributed to the above-mentioned reason. For dye degradation by cerium ion-doped TiO_2 hydrosol under visible illumination, Xie and Yuan [15] pointed out the four proposed mechanisms: (I) photolysis mechanism; (II) photosensitization mechanism for TiO_2 nanocrystallites system; (III) photosensitization mechanism for cerium ion-doped TiO_2 hydrosol system; and (IV) interband photocatalysis mechanism for cerium ion-doped TiO_2 nanocrystallites. In this study, the MB degradation with pure TiO_2 hydrosol under visible illumination should obey the mechanisms (I) and (II). The "Blank" (without catalyst) and "Pure TiO_2" in Fig. 5b may represent the photolysis and photosensitization, respectively. However, since these two reaction rates were very slow, the photolysis (I) and photosensitization (II) in the Ce^{3+}-TiO_2/MB system under visible illumination could be ignored. Therefore, the MB degradation with Ce^{3+}-TiO_2 hydrosol under visible illumination might be dominated by the mechanisms (III) and (IV), and the interband Ce 4*f* levels lead the enhanced visible-response photocatalytic activity for MB degradation.

Since 2,3-DCP had no significant absorption of either UVA or visible light. The 2,3-DCP degradation with Ce^{3+}-TiO_2 hydrosols should mainly result from the mechanism (IV). However, it has been noted that 2,3-DCP was degraded by the pure TiO_2 hydrosol under visible illumination with *k* value significantly higher than that of "Blank". This result demonstrated that the pure TiO_2/2,3-DCP system had certain visible-response. Agrios et al. [20, 21] observed that 2,4,5-trichlorophenol formed a charge-transfer complex on TiO_2 and correlated the charge transfer surface complex formation with visible light absorption among several chlorophenols. They pointed

out that surface complex formation on pure TiO_2 was responsible for the visible-light-induced photocatalytic transformation of substrates that do not absorb visible photons by them alone. Choi et al. [22] demonstrated that 4-chlorophenol, as one of the most common substrates used in many studies of photocatalytic degradation, can be actually degraded and mineralized under visible irradiation ($\lambda > 420$ nm). The visible light reactivity of 4-chlorophenol was correlated with the surface complex formation that was supported by the diffuse reflectance UV-Vis spectra and visible-light-induced photocurrent generation. Other phenolic compounds showed similar visible light reactivity. Since 2,3-DCP is a member of phenolic compounds, the mechanisms of 2,3-DCP degradation with Ce^{3+}-TiO_2 hydrosol under visible illumination should include the Ce 4*f* level function as the interband photocatalysis mechanism and plus the charge transfer surface complex formation. It should be noted that the $\cdot O_2^-$ can be generated through O_2 capturing the electrons in two ways: (i) the electron of Ce-TiO_2 was directly irradiated to Ce 4*f* level under visible light illumination; (ii) the electron of TiO_2-DCP complex was transferred to conduction band of TiO_2, so the $\cdot O_2^-$ can also contribute to the 2,3-DCP degradation. The possible reaction mechanisms of 2,3-DCP degradation with Ce^{3+}-TiO_2 hydrosol under visible illumination are summarized in Fig. 7.

[Fig. 7]

3.4 Photocatalytic activity in gaseous phase

To evaluate the effects of Ce^{3+} content on the photocatalytic activity of Ce^{3+}-TiO_2 hydrosols in gaseous phase, two sets of tests for degradations of gaseous benzene with different catalysts under UVA and visible illumination were conducted. The experimental results in Fig. 8 showed that the photocatalytic activity of Ce^{3+}-TiO_2 hydrosols for benzene degradation in gaseous phase was also significantly affected by the Ce^{3+} content. From the kinetic data shown in Fig. 8c, the results indicated that the benzene degradation under UVA or visible illumination both increased with the increase of Ce^{3+} content initially, but declined while the Ce^{3+} content reached 1.0%, and this was well consistent with the results of MB and 2,3-DCP degradation in aqueous phase.

[Fig. 8]

It is found that the benzene degradation by pure TiO_2 hydrosol under visible illumination was so weak that can be ignored. Based on the above-mentioned mechanisms, the benzene photodegradation by Ce^{3+}-TiO_2 hydrosols was attributed to neither the photolysis nor the photosensitization of TiO_2-benzene system. The enhancement of electron-hole pair separation owing to lanthanide ion doping was previously proved by the PL emission spectra [23], as a result of the enhanced activity for BTEX degradation. Hence, it can be concluded that the enhanced photocatalytic activity by Ce^{3+} doping under UVA or visible illumination should be dominated by the mechanism (IV): the interband Ce 4*f* levels lead higher electron-hole separating efficiency and enhanced visible light response.

Besides, it is well known that the large surface area is favorable to the photocatalytic reaction, but in this study, the benzene degradation did not depend on the BET surface areas very much. To illustrate the reasons, we briefly reviewed the Langmuir-Hinshelwood approach [24] that assumes one reaction achieving adsorption equilibrium ($R_{gas} \rightarrow R_{ads}$) is followed by a single surface reaction step ($R_{ads} \rightarrow products$) illustrated by the following equation:.

$$R_{gas} \xrightarrow{adsorprtio\ n} R_{ads} \xrightarrow{photo\ \deg\ radation} products$$

wherein the R_{gas} and R_{ads} represent the gaseous reactant and the adsorbed reactant, respectively. The adsorption rate of $R_{gas} \rightarrow R_{ads}$ is defined as r_{ads}, and the photodegradation rate of $R_{ads} \rightarrow products$ is defined as r_{pd}. Hence, when the $r_{ads} < r_{pd}$, the adsorption step ($R_{gas} \rightarrow R_{ads}$) should be the rate-determining step (RDS); in contrast, when the $r_{ads} > r_{pd}$, the photodegradation ($R_{ads} \rightarrow products$) should be the RDS. The values of adsorption rate constants for benzene on pure TiO_2 were calculated (data not shown in figure) to be 0.1887 h^{-1} (R^2=0.8693), which was significantly higher than the *k* values in Fig. 8c, indicating that the slow photodegradation step should be the RDS under. Hence, this might be the reason why the rate of benzene degradation by Ce^{3+}-TiO_2 hydrosols under our experimental conditions was not affected by the BET surface areas significantly.

Conclusions

The Ce^{3+}-TiO_2 hydrosols with Ce^{3+} content from 0% to 1.5% as stable colloid solutions were successfully prepared by a coprecipitation–peptization method. The characteristics of these

hydrosols demonstrated that as the Ce^{3+} content increased, the crystalline size, the BET surface area and transmittance decreased significantly, but the particle size increased. The results showed that the overall photocatalytic activity of Ce^{3+}-TiO_2 hydrosols for MB and 2,3-DCP degradations in aqueous phase under UVA and visible illumination was significantly higher than pure TiO_2 hydrosol due to the Ce 4*f* level-induced better separation of electron-hole pairs and visible light response. Additionally, the formation surface-complex of TiO_2 and 2,3-DCP with visible-light-response also contributed to the 2,3-DCP degradation. The experiments also confirmed that the Ce^{3+}-TiO_2 hydrosols had the higher activity for benzene degradation in gaseous phase under UVA and visible illumination. The 0.5-1%Ce^{3+}-TiO_2 hydrosols achieved the best performance in both of aqueous and gaseous phases.

Acknowledgements

The authors would thank the Hong Kong Government Research Grant Committee for a financial support to this work (RGC No: PolyU 5226/06E).

References

[1] U.I. Gaya, A.H. Abdullah, Heterogeneous photocatalytic degradation of organic contaminants over titanium dioxide: A review of fundamentals, progress and problems, J. Photochem. Photobiol. C 9 (2008) 1-12.

[2] K. Demeestere, J. Dewulf, H. Van Langenhove, Heterogeneous photocatalysis as an advanced oxidation process for the abatement of chlorinated, monocyclic aromatic and sulfurous volatile organic compounds in air: State of the art, Crit. Rev. Environ. Sci. Technol. 37 (2007) 489-538.

[3] N.I. Al-Salim, S.A. Bagshaw, A. Bittar, T. Kemmitt, A.J. McQuillan, A.M. Mills, M.J. Ryan, Characterisation and activity of sol-gel-prepared TiO_2 photocatalysts modified with Ca, Sr or Ba ion additives, J. Mater. Chem. 10 (2000) 2358-2363.

[4] T. Kawahara, T. Ozawa, M. Iwasaki, H. Tada, S. Ito, Photocatalytic activity of rutile-anatase coupled TiO_2 particles prepared by a dissolution-reprecipitation method, J. Colloid Interf. Sci. 267 (2003) 377-381.

[5] D.H. Kuo, C.N. Shueh, Growth and properties of $TiCl_4$-derived CVD titanium oxide films at

various C-2/H-2 inputs, Chem. Vap. Deposit. 9 (2003) 265-271.

[6] Y.B. Xie, C.W. Yuan, Photocatalytic activity and recycle application of titanium dioxide sol for X-3B photodegradation, J. Mol. Catal. A. 206 (2003) 419-428.

[7] T.X. Liu, F.B. Li, X.Z. Li, TiO_2 Hydrosols with high activity for photocatalytic degradation of formaldehyde in a gaseous phase, J. Hazard. Mater. 152 (2007) 347-355.

[8] T.X. Liu, F.B. Li, X.Z. Li, Effects of peptizing conditions on nanometer properties and photocatalytic activity of TiO_2 hydrosols prepared by H_2TiO_3, J. Hazard. Mater. 155 (2008) 90-99.

[9] Y.Q. Wang, H.M. Cheng, Y.Z. Hao, J.M. Ma, W.H. Li, S.M. Cai, Photoelectrochemical properties of metalion-doped TiO_2 nanocrystalline electrodes, Thin Solid Films 349 (1999) 120-125.

[10] W. Xu, Y. Gao, H.Q. Liu, The preparation,characterization, and their photocatalytic activities of rare-earthdoped TiO_2 nanoparticles, J. Catal. 207 (2002) 151-157.

[11] W.Y. Su, E.X. Chen, L. Wu, X.C. Wang, X.X. Wang, X.Z. Fu, Visible light photocatalysis on praseodymium(III)-nitrate-modified TiO_2 prepared by an ultrasound method, Appl. Catal. B 77 (2008) 264-271.

[12] Z.M. Shi, L.N. Jin, Influence of La^{3+}/Ce^{3+}-doping on phase transformation and crystal growth in TiO_2-15wt% ZnO gels, J. Non-Crystal. Solids 355 (2009) 213-220.

[13] C.H. Liang, C.S. Liu, F.B. Li, F. Wu, The effect of Praseodymium on the adsorption and photocatalytic degradation of azo dye in aqueous Pr^{3+}-TiO_2 suspension, Chem. Eng. J. 147 (2009) 219-225.

[14] F.B. Li, X.Z. Li, M.F. Hou, K.W. Cheah, W.C.H. Choy, Enhanced photocatalytic activity of Ce^{3+}-TiO_2 for 2-mercaptobenzothiazole degradation in aqueous suspension for odour control, Appl. Catal. A 285 (2005) 181–189.

[15] Y.B. Xie, C.W. Yuan, Visible-light responsive cerium ion modified titania sol and nanocrystallites for X-3B dye photodegradation, Appl. Catal. B 46 (2003) 251–259.

[16] J.H. Huang, X.C. Wang, Y.D. Hou, X.F. Chen, L. Wu and X.Z. Fu, Degradation of benzene over a zinc germanate photocatalyst under ambient conditions, Environ. Sci. Technol. 42 (2008) 7387-7391.

[17] J.G. Yu, G.H. Wang, B. Cheng and M.H. Zhou, Effects of hydrothermal temperature and time on the photocatalytic activity and microstructures of bimodal mesoporous TiO_2 powders, Appl. Catal. B 69 (2007) 171-180.

[18] S.L. Gregg, K.S.W. Sing, Adsorption, surface area and porosity, Academic Press, London, 1982.

[19] K.T. Ranjit, I. Willner, S.H. Bossmann, A.M. Braun, Lanthanide oxide-doped titanium dioxide photocatalysts: Novel photocatalysts for the enhanced degradation of p-chlorophenoxyacetic acid, Environ. Sci. Technol. 35 (2001) 1544-1549.

[20] A.G. Agrios, K.A. Gray, E. Weitz, Photocatalytic transformation of 2,4,5-trichlorophenol on TiO_2 under sub-band-gap illumination, Langmuir 19 (2003) 1402-1409.

[21] A.G. Agrios, K.A. Gray, E. Weitz, Narrow-band irradiation of a homologous series of chlorophenols on TiO_2: Charge-transfer complex formation and reactivity, Langmuir 20 (2004) 5911-5917.

[22] S.H. Kim, W.Y. Choi, Visible-light-induced photocatalytic degradation of 4-Chlorophenol and phenolic compounds in aqueous suspension of pure titania: demonstrating the existence of a surface-complex-mediated path, J. Phys. Chem. B 109 (2005) 5143-5149.

[23] F.B. Li, X.Z. Li, C.H. Ao, S.C. Lee, M.F. Hou, Enhanced photocatalytic degradation of VOCs using Ln^{3+}-TiO_2 catalysts for indoor air purification, Chemosphere 59 (2005) 787-800.

[24] D.F. Ollis, Kinetics of liquid phase photocatalyzed reactions: an illuminating approach, J. Phys. Chem. B 109 (2005) 2439-2444.

Tables

Table 1 The ratios of sol to precipitate and UV-Visible transmittance

Ce^{3+} content (%)	0	0.5%	1.0%	1.5%	2.0%	2.5%
Sol/ Precipitate* wt%	100 / 0	100 / 0	100 / 0	82.7 / 17.3	2.9 / 97.1	0 / 100
Transmittance# T%	77.41	76.91	67.15	48.91	>90	>98

"Sol/ Precipitate*" means the dry weight ratio of the solid titania in the obtained sol to the titania precipitate which wasn't transformed into sol by weighing the solid titania in the liquid before and after filtration, respectively, and then calculating.

"Transmittance#" represents the transmittance of the hydrosol (the ratio of solid 0.05 wt%) at the wavelength of 600 nm.

1 Table 2 The crystal size, particle size, surface area, pore volume, pore size of catalysts

Catalysts	Crystallite Size nm	Surface Area $m^2 g^{-1}$	Particle Size nm	Pore Size nm	Pore Volume $cm^3 g^{-1}$
Pure TiO_2	12.95	379.02	26.3	5.27	0.499
0.5%Ce^{3+}-TiO_2	12.14	330.72	27.9	5.18	0.429
1.0%Ce^{3+}-TiO_2	11.60	245.45	30.2	5.39	0.331
1.5%Ce^{3+}-TiO_2	10.38	158.68	32.8	5.29	0.210

2

Figure captions:

Fig. 1. The transmittance of pure TiO_2 hydrosol and Ce^{3+}-TiO_2 hydrosols

Fig. 2. The particle size distributions of different pure TiO_2 hydrosol and Ce^{3+}-TiO_2 hydrosols

Fig. 3. The XRD patterns of pure TiO_2 hydrosol and Ce^{3+}-doped TiO_2 hydrosols

Fig. 4. (a) The N_2 adsorption-desorption isotherms of pure TiO_2 hydrosol and Ce^{3+}-doped TiO_2 hydrosols; (b) The pore size distributions of pure TiO_2 hydrosol and Ce^{3+}-doped TiO_2 hydrosols

Fig. 5. The MB degradation by pure TiO_2 and Ce^{3+}-TiO_2 hydrosols (a) under UVA illumination; (b) under visible illumination; (c) the apparent kinetic constant, k vs. cerium ion content

Fig. 6. The 2,3-DCP degradation by pure TiO_2 and Ce^{3+}-TiO_2 hydrosols (a) under UVA illumination; (b) under visible illumination; (c) the apparent kinetic constant, k vs. cerium ion content

Fig. 7. The proposed valence band structure of Ce^{3+}-TiO_2 and the mechanisms of photoresponse under visible light and photogenerated electron transfer in Ce^{3+}-TiO_2/2,3-DCP system

Fig. 8. The benzene degradation by pure TiO_2 and Ce^{3+}-TiO_2 hydrosols (a) under UVA illumination; (b) under visible illumination; (c) the apparent kinetic constant, k vs. cerium ion content

Fig. 1.

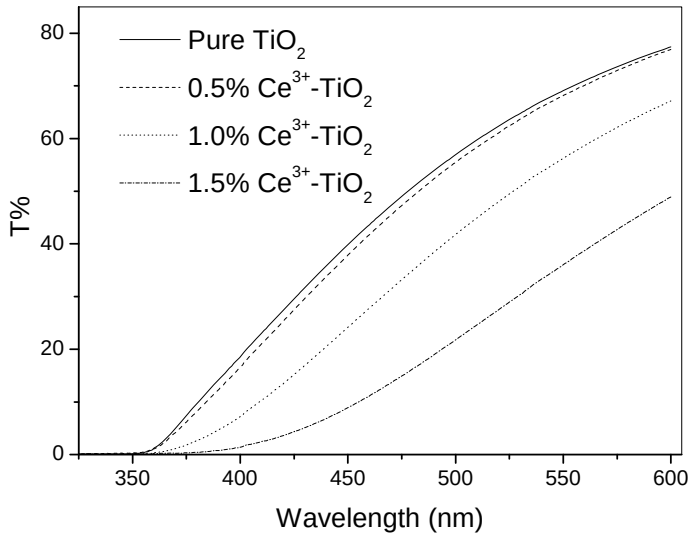
Pure TiO2
0.5% Ce3+-TiO2
1.0% Ce3+-TiO2
1.5% Ce3+-TiO2
T%
Wavelength (nm)
0
20
40
60
80
350
400
450
500
550
600

Fig. 2.

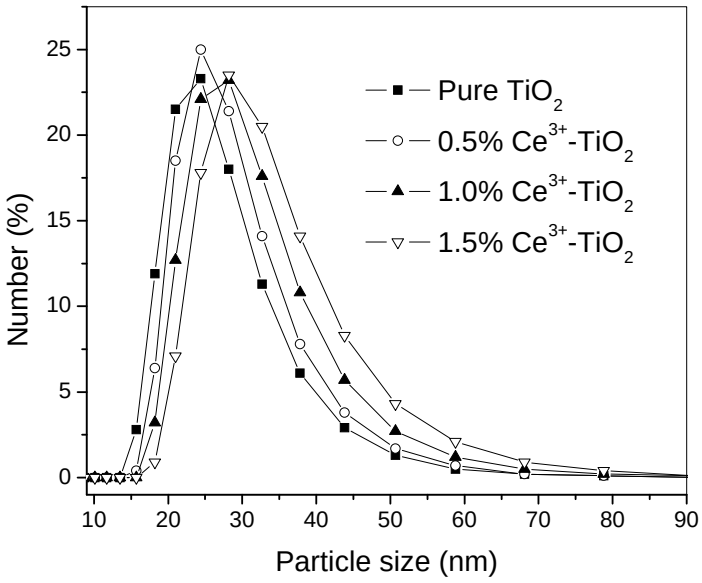
Number (%)
Particle size (nm)
Pure TiO2
0.5% Ce3+-TiO2
1.0% Ce3+-TiO2
1.5% Ce3+-TiO2

1 **Fig. 3.**

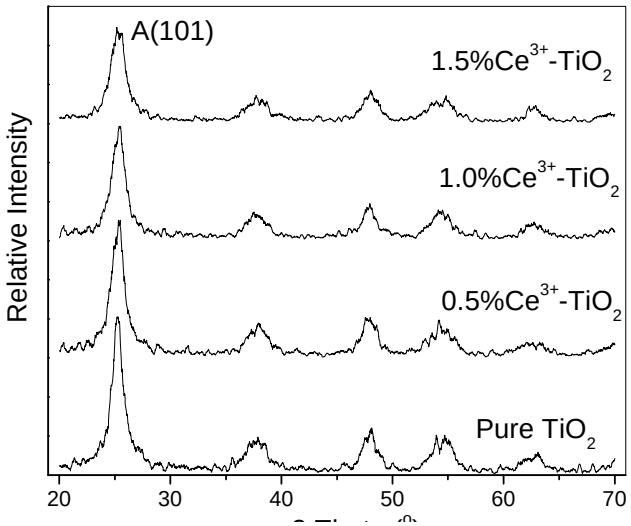
A(101)
1.5%Ce3+-TiO2
1.0%Ce3+-TiO2
0.5%Ce3+-TiO2
Pure TiO2
Relative Intensity
20
30
40
50
60
70

2

Fig. 4.

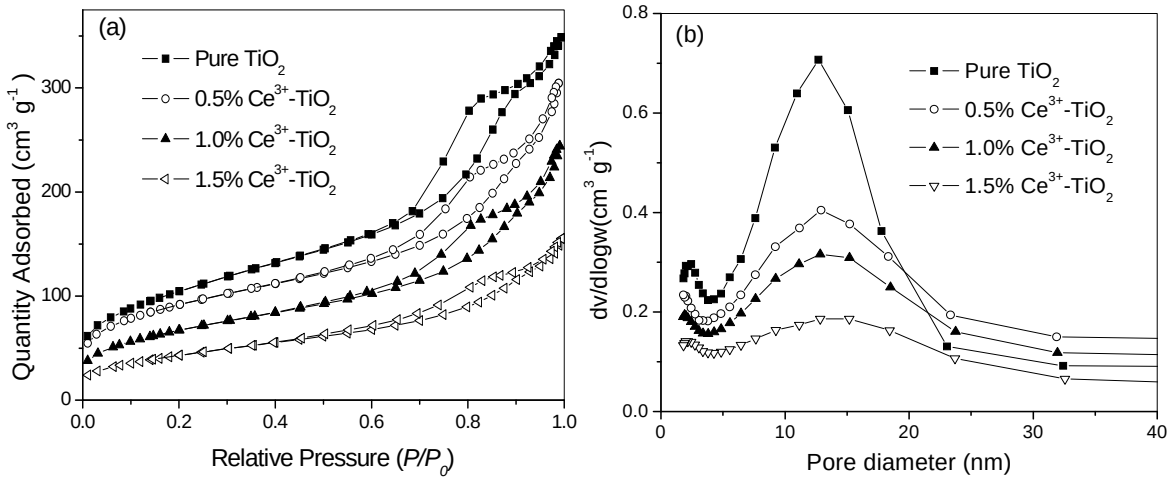
(a)
Pure TiO2
0.5% Ce3+-TiO2
1.0% Ce3+-TiO2
1.5% Ce3+-TiO2
Quantity Adsorbed (cm3 g-1)
Relative Pressure (P/P0)
(b)
dv/dlogw(cm3 g-1)
Pore diameter (nm)

Fig. 5.

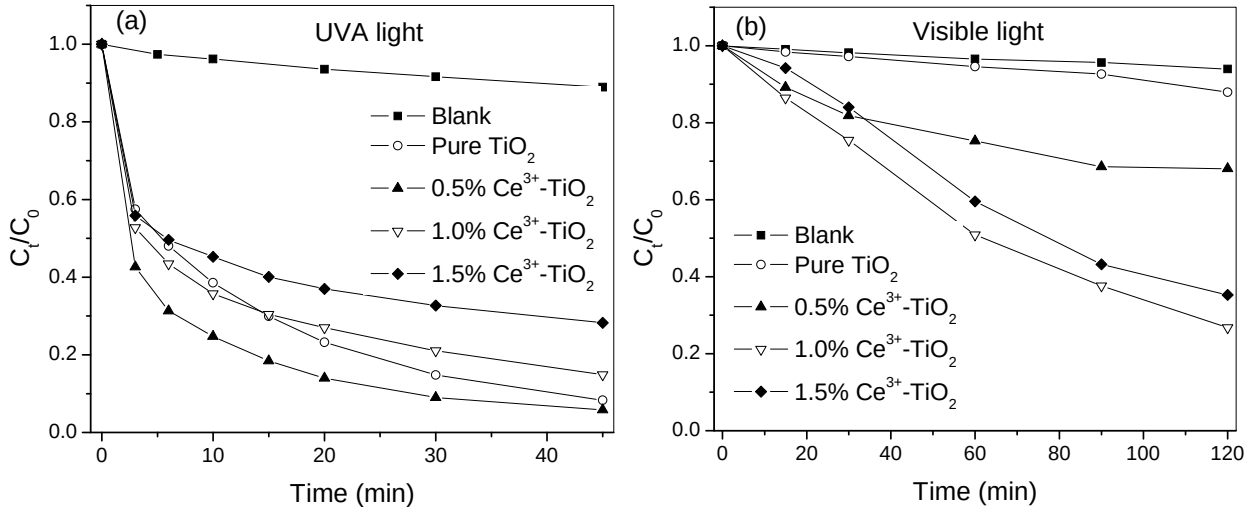
(a)
UVA light
Blank
Pure TiO2
0.5% Ce3+-TiO2
1.0% Ce3+-TiO2
1.5% Ce3+-TiO2
Ct/C0
Time (min)
(b)
Visible light
Blank
Pure TiO2
0.5% Ce3+-TiO2
1.0% Ce3+-TiO2
1.5% Ce3+-TiO2
Ct/C0
Time (min)

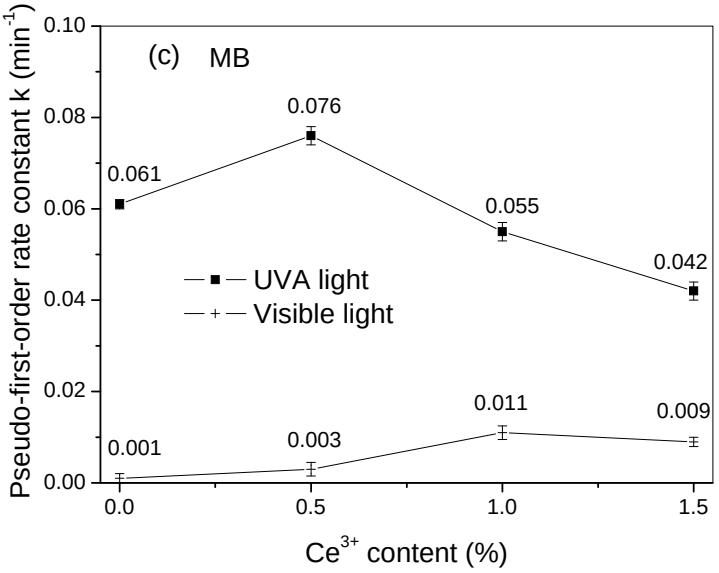
(c) MB
Pseudo-first-order rate constant k (min-1)
UVA light
Visible light
0.061
0.076
0.055
0.042
0.001
0.003
0.011
0.009
Ce3+ content (%)

Fig. 6.

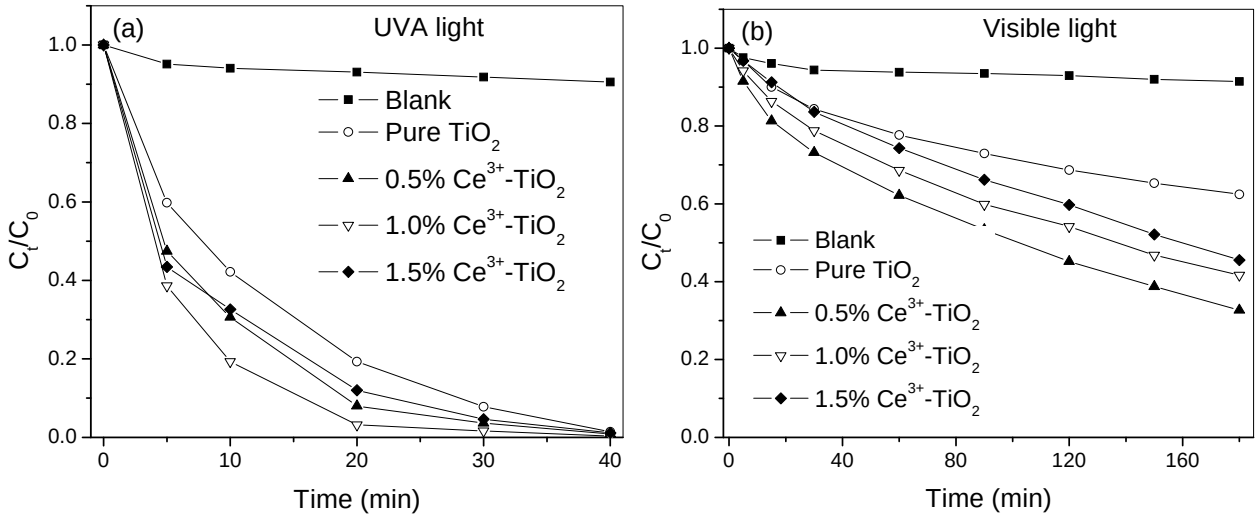
(a)
UVA light
Blank
Pure TiO2
0.5% Ce3+-TiO2
1.0% Ce3+-TiO2
1.5% Ce3+-TiO2
Ct/C0
Time (min)
(b)
Visible light
Blank
Pure TiO2
0.5% Ce3+-TiO2
1.0% Ce3+-TiO2
1.5% Ce3+-TiO2
Ct/C0
Time (min)

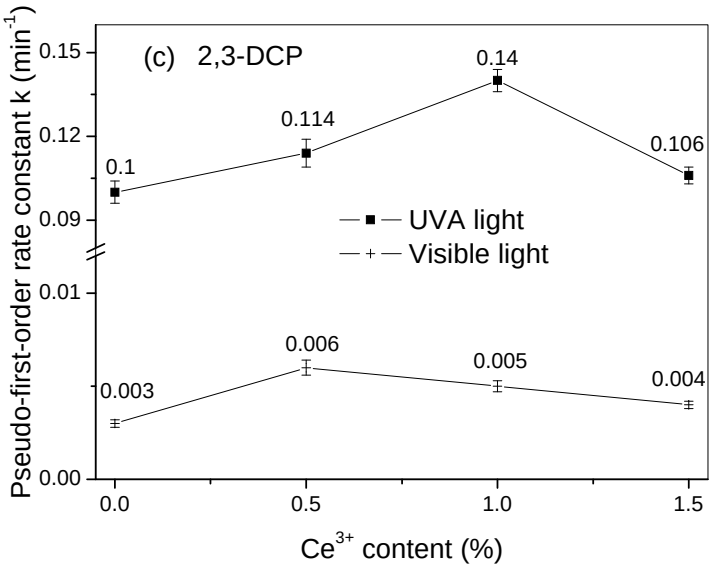
(c) 2,3-DCP
UVA light
Visible light
0.1
0.114
0.14
0.106
0.003
0.006
0.005
0.004
Pseudo-first-order rate constant k (min-1)
Ce3+ content (%)

Fig. 7.

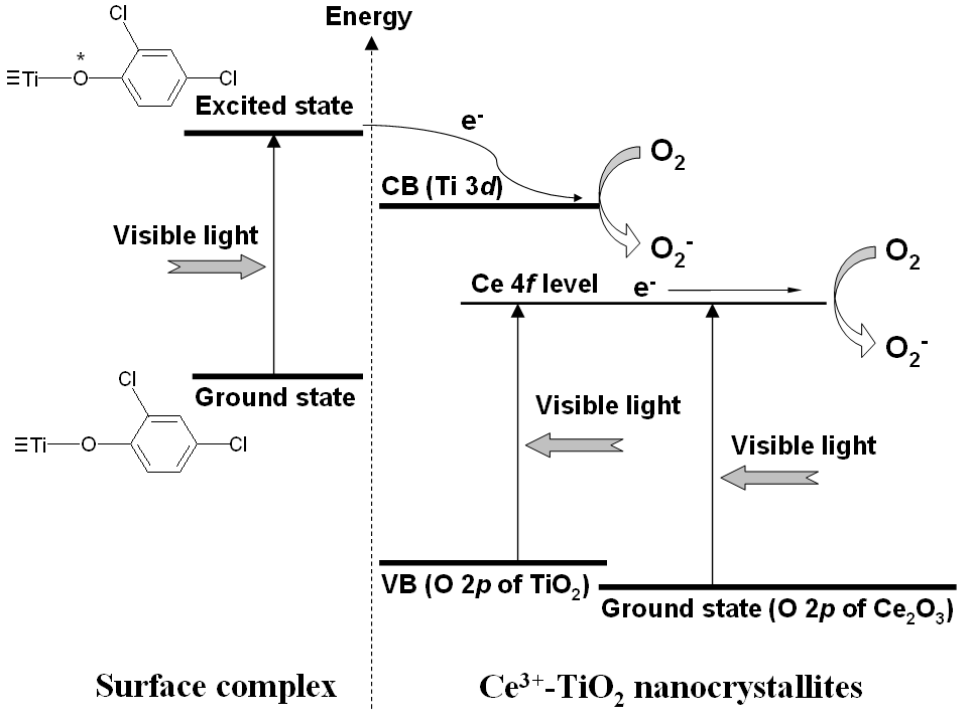
Energy
Excited state
e-
CB (Ti 3d)
O2
O2-
Visible light
Ce 4f level
e-
O2
O2-
Ground state
Visible light
Visible light
VB (O 2p of TiO2)
Ground state (O 2p of Ce2O3)
Surface complex
Ce3+-TiO2 nanocrystallites

Fig. 8.

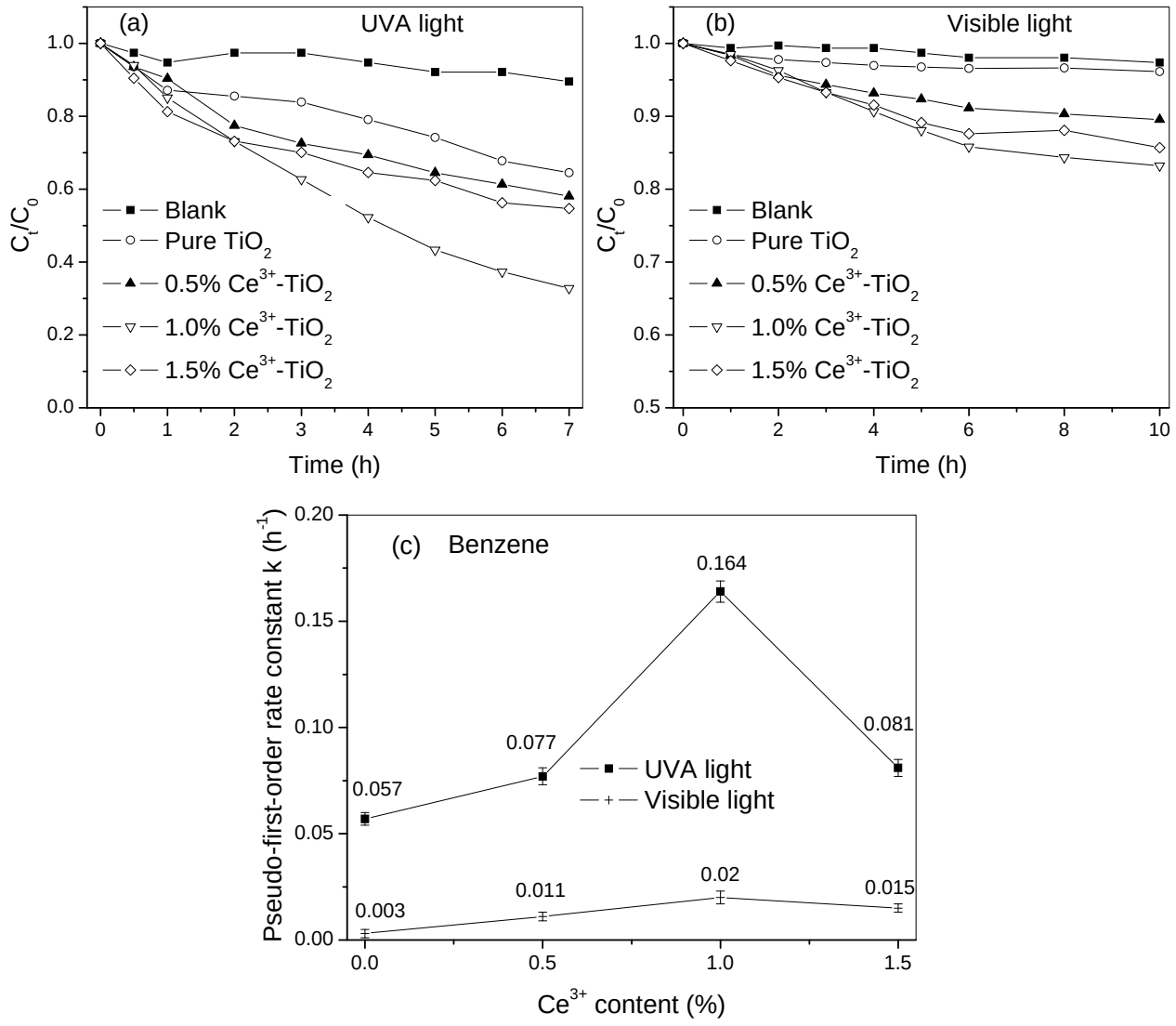
(a)
UVA light
C_t/C_0
Time (h)
Blank
Pure TiO_2
0.5% Ce^{3+}-TiO_2
1.0% Ce^{3+}-TiO_2
1.5% Ce^{3+}-TiO_2
(b)
Visible light
C_t/C_0
Time (h)
Blank
Pure TiO_2
0.5% Ce^{3+}-TiO_2
1.0% Ce^{3+}-TiO_2
1.5% Ce^{3+}-TiO_2
(c) Benzene
Pseudo-first-order rate constant k (h^{-1})
Ce^{3+} content (%)
UVA light
Visible light
0.057
0.077
0.164
0.081
0.003
0.011
0.02
0.015